Z. Phys. C – Particles and Fields 51, 209–224 (1991)

Zeitschrift für Physik C Particles and Fields

The spectral analysis of strongly interacting matter

F. Karsch, H. Satz
Theory Division, CERN, CH-1211 Geneva 23, Switzerland and
Fakultät für Physik, Universität Bielefeld, W-4800 Bielefeld, Federal Republic of Germany

Received 4 February 1990

Abstract. The intensity of spectral lines in the light emitted by stars gives information about the thermodynamic state of stellar matter. Similarly, the intensity of charmonium and bottonium lines in the spectrum of dileptons emitted in nuclear collisions can provide information about the early thermodynamic state of any strongly interacting matter created in such collisions. The J/ψ suppression found in central $O-U$ and $S-U$ collisions is a first instance of a change in spectral intensity. We develop a full spectral analysis for the production of $c\bar{c}$ and $b\bar{b}$ resonances and discuss how it can be used to explore the primordial state of matter produced in high energy heavy ion collisions.

1 Introduction

How can we measure the temperature of the bubbles of strongly interacting matter produced in high energy heavy ion collisions? What tells us whether the interior of such "hot" bubbles forms a plasma of deconfined quarks and gluons? These questions have attracted an increasing interest over the past years, much stimulated by the advent of data for so far rather light ions (O, Si, S), incident on heavy ion targets, from CERN and BNL [1].

The generally proposed "thermometers" are direct photons and thermal dileptons [2]; they should escape from the interior at an early time, without effects from the outer layers or later hadronisation. So far, however, both have proved to be not so easily accessible. It is difficult to find direct photons under the strong background from meson decays [3], and thermal dileptons in the interesting mass range ($M_{l^+l^-} \geqq 2$ GeV) may always remain hidden under pairs from hadron decays or under the Drell-Yan continuum [4].

On the other hand, the suppression of the J/ψ signal relative to the Drell-Yan continuum, predicted as indication of quark deconfinement [5, 6], is experimentally indeed observed [7–11]. At present it is not clear, however, if this effect is really first evidence for quark-gluon plasma formation; it could also be due to absorption in dense hadronic matter [12–20], and further checks as well as more precise data are needed to determine its origin. But both accounts require the presence of a dense, strongly interacting medium, and so J/ψ suppression does tell us something about the nature of the system produced in high energy heavy ion collisions.

The aim of this paper is to propose a general framework for determining the thermodynamic state of the bubbles of dense matter produced in heavy ion collisions. Our scheme will in particular also provide tests of the origin of J/ψ suppression, based on the different finite space-time features of suppression by colour screening [6, 21–24] and by absorption [12–17]. In the case of colour screening, the inherent features accommodate quite well the dependence of the suppression on the associated hadron production (E_T) as well as on the transverse momentum of the J/ψ [21–24]. In the absorption approach, the effect of initial state parton scattering has to be added to describe correctly the observed suppression pattern [18–20]. We want to study here the further implications of the finite space-time extension of the produced high density system on other charmonium and bottonium states, and we want to see if they lead to observable differences between colour deconfinement and absorption as origins for the observed suppression.

The basis for our considerations is the same as that used in astrophysics to determine the temperature of stellar matter [25], and it seems instructive to elaborate this point a little. A star is a hot gas of atoms of different elements in various stages of excitation and of ionisation. These emit and absorb radiation corresponding to the transition frequencies between the different excitation levels – radiation observed in form of spectral lines of certain intensities. In a "hotter" star, containing fewer atoms in low excitation levels, the intensity of the spectral lines from such lower excitation levels will be reduced ("become suppressed"). In the limit of sufficiently high temperatures, all atoms will become fully ionised ("all bound states are completely suppressed"), and there are no more spectral lines, but only radiation from a continuum of unbound charged constituents. Similarly, as we shift from the outer layers of a star to its interior, the degree of ionization increases. The analysis of stellar spectra thus provides us with information about the state and the temperature of stellar matter.

In the case of strongly interacting matter, the prediction of J/ψ suppression is only the first step in such a spectral analysis; it corresponds to noting that with increasing temperature, the spectral line corresponding to the transition from the ground state to the first excited state of the hydrogen atom should decrease in intensity. Similar predictions apply to higher $c\bar{c}$ and to $b\bar{b}$ states as well, opening the way to a much more complete analysis. The origin of bound state suppression in strongly interacting matter still has to be determined. Absorption provides a break-up mechanism similar to the ionisation in stellar matter, with break-up cross sections taking the place of ionisation energies. But even for a quark-gluon plasma, where the mechanism leading to the suppression is quite different (colour charge screening instead of ionisation), we can still make use of the fate of heavy quark bound states in a deconfining medium to determine the state of that medium. By comparing the suppression pattern of the J/ψ to that of other, higher mass bound states of heavy quarks (ψ', χ, Υ, Υ') as function of the thermodynamic and kinematic variables, we will obtain a scheme for investigating the primordial state of the strongly interacting matter produced in heavy ion experiments.

Why should we restrict this analysis to $c\bar{c}$ and $b\bar{b}$ bound states? In contrast to the analysis of genuine stellar matter, we are here faced with a "star" which is rapidly expanding and cooling, and we want information about its early stages, before hadronisation. Hence we have to study bound states produced at a very early time, and only then: they must be decoupled from the thermodynamics, which destroys the memory of the history of the system. The lighter $q\bar{q}$ states, presumably in thermal equilibrium, will therefore in general provide information only about the hadronisation era.

This paper is organized as follows. In Sect. 2, we review the space-time restrictions for suppression by colour screening and by absorption in dense matter. In Sect. 3, we then show the effect of these restrictions for idealized systems of very large spatial size or very large lifetime. After discussing in Sect. 4 the conditions to be expected in actual nuclear collisions, we present in Sect. 5 the predicted suppression patterns for charmonium and bottonium formation at SPS, RHIC and LHC energies. In Sect. 6 we consider the experimental conditions necessary for the spectral analysis proposed here, and finally, in Sect. 7, we summarize the main features that could be used to distinguish between deconfinement and absorption as suppression mechanisms.

2 Space-time restrictions on suppression of heavy quark bound states

We begin by recalling how the two different mechanisms mentioned – colour screening and absorption – lead to a suppression of the signal from heavy quark bound states in the spectrum of dileptons emitted in high energy heavy ion collisions.

Within a deconfining medium, quarks cannot bind to form hadrons. If a heavy ion collision produces such a medium, then this subsequently expands, cools off, and after passing the confinement temperature T_c, it hadronises: the quarks and antiquarks now combine to form mesons and baryons. Heavy quark-antiquark pairs ($c\bar{c}$, $b\bar{b}$) are produced by hard, pre-thermal interactions (gluon fusion) at a very early stage of the collision. In a confining medium, such as the physical vacuum, they subsequently are bound by the confining potential to form charmonium (ψ, χ_c, ψ') or bottonium (Υ, χ_b, Υ') states*. In a deconfining medium, colour screening prevents this binding, and so the c and the $\bar{c}$ (or the b and the $\bar{b}$) just "fly apart". At hadronisation, the thermal production of additional heavy quarks is very strongly suppressed; hence the separated partners of the heavy quark pair must then combine with light quarks to form states of open charm or beauty instead of heavy quark bound states [5].

In the absorption approach, one assumes that a charmonium or bottonium state produced in the very early stages of a nuclear collision finds itsself shortly afterwards in a very dense medium of hadronic constituents; consider the ψ for illustration. When it collides with the constituents of its dense environment, it can be broken up by reactions of the type

$$\psi + h \to D + \bar{D} + X, \tag{1}$$

and this will reduce the signal in the spectrum of dileptons from dense hadronic matter, in comparison to that from less dense matter or from hadron-hadron collisions [12–17]. If the constituents of the dense hadronic environment are pions, reaction (1) can only take place for sufficiently energetic ψ's, since $2m_D - m_\psi \simeq 650$ MeV. Including hadronic resonances such as ρ's will, however, reduce this threshold effect [14, 15]. Conceptually, absorption differs from screening in that now the break-up occurs locally, is caused by the interaction of the ψ with one of the constituents of the dense medium; colour screening, in contrast, is a global effect, due to the medium as a whole.

For both mechanisms the suppression ends when the medium has cooled off sufficiently. The resulting limits are quite different, however. Screening stops when the temperature of the medium has dropped to a value lower than that needed to melt the bound state; absorption, on the other hand, stops much later, when the system has become so dilute that there are no more interactions.

Any system of dense matter produced in a heavy ion collision will thus have a finite life-time as well as a finite spatial size. This makes it possible for a $c\bar{c}$ or $b\bar{b}$ pair of sufficient momentum to escape from the medium before suffering any suppression effect. In the deconfinement approach, if the two quarks have separated less than the radius of the bound state in question when they leave the deconfining medium (either spatially or because the medium has cooled off beyond the point

* We shall here designate by ψ the directly produced $1S$ $c\bar{c}$ state, and by J/ψ the signal actually observed in the dilepton spectrum, of which at cms energy $\sqrt{s} = 20$ GeV about 60% is directly produced and about 40% comes from χ_c decay [26]. At higher energies, however, this fraction will change [27], and we shall therefore consider the different bound states separately

where it can screen the binding potential), formation of the bound state can still occur and there will be no suppression. In the absorption approach, the two quarks must also separate up to the radius of the bound state before we can talk about a break-up of the state by reactions of the form (1); if they have left the dense hadronic medium before that is the case, there will not be absorption due to genuine hadron-hadron interaction. In both cases, we have assumed a well-defined bound state "formation time" [23, 28], governing the onset of deconfinement or absorption; this is clearly on oversimplification. Screening will have an effect on the evolution of the bound state even before it has reached its full size [29–31], and a "pre-hadronic" bound state can also interact already with the constituents of a dense hadronic medium [32]. The inclusion of such effects will lead to earlier and stronger suppression. To keep our arguments as simple and transparent as possible, we shall nevertheless retain the idea of a definite formation time and return later to the consequences of a more detailed description.

Let us then try to estimate the time needed, after the production of the heavy quark pair, to form a bound state; we take again the ψ as example. Its radius is from charmonium spectroscopy [33] known to be $r_\psi \simeq 0.45$ fm; the momentum of each quark in the ψ is $p_\psi \simeq 0.67$ GeV [23]. Thus the time τ_ψ, which the $c\bar{c}$ pair needs in its own rest-frame to separate in free flight the distance r_ψ, is

$$\tau_\psi = m_c\, r_\psi / p_\psi \simeq 0.89 \text{ fm}, \tag{2}$$

with $m_c = 1.32$ GeV for the mass of the c-quark [33]. In the same way, one can obtain the formation times also for the other heavy quark bound states [23]; they are listed in Table 1.

In the rest-frame of the medium, the time τ_ψ becomes

$$t_\psi = \tau_\psi (1 + \mathbf{P}^2/M_\psi^2)^{1/2}, \tag{3}$$

with $\mathbf{P}$ denoting the three momentum of the $c\bar{c}$ pair. During the time τ_ψ, the pair will have moved a distance

$$s_\psi = \tau_\psi (|\mathbf{P}|/M_\psi), \tag{4}$$

away from its production point, measured in the overall rest-frame. If

$$t_\psi \geqq t_\psi^d, \tag{5}$$

where t_ψ^d is the time at which the medium has become too cold to screen the ψ binding potential, or too dilute to lead to break-up through collisions, then the $c\bar{c}$ pair has escaped; it will become a ψ, and we have no suppression. Similarly, if

$$s_\psi \geqq R_d, \tag{6}$$

where R_d is the radius of the bubble of dense matter, then on the average a $c\bar{c}$ or $b\bar{b}$ pair will still be "together" when it leaves the medium, and hence there will be no suppression. In condition (6), we have neglected the expansion of the medium, which can be justified at most in the transverse direction; hence we can only use it to obtain finite size restriction on the transverse momentum of the ψ.

Table 1. Bound state masses M_x [GeV], radii r_x [fm], formation times τ_x [fm], critical screening masses μ_x [GeV], dissociation temperatures T_x^d and break-up cross sections σ_x [fm^2], for $c\bar{c}$ and $b\bar{b}$ states. The dissociation temperatures are given in terms of the deconfinement temperature $T_c = 150$ MeV; the cross sections were obtained using geometric arguments [39] and $\sigma_\psi = 0.1$ fm$^2 = 1$ mb

States	ψ	ψ'	χ_c	Υ	Υ'	χ_b
M_x	3.1	3.7	3.5	9.6	10.0	9.9
r_x	0.45	0.88	0.70	0.23	0.51	0.41
τ_x	0.89	1.5	2.0	0.76	1.9	2.6
μ_x	0.70	0.36	0.34	1.57	0.67	0.56
T_x^d/T_c	1.17	1.0	1.0	2.62	1.12	1.0
σ_x	0.1	0.37	0.24	0.025	0.13	0.08

From (3) and (5), we get a limiting transverse momentum for the ψ,

$$P_\psi^d = M_\psi [(t_\psi^d/\tau_\psi)^2 - 1]^{1/2}, \tag{7}$$

with no more suppression for $P_T^\psi \geqq P_\psi^d$. A restriction due to the finite life-time of the dense medium can also be obtained for longitudinal momenta (see [34]); we shall here consider only transverse momenta.

From (4) and (6), the transverse momentum of the ψ is restricted to be less than

$$P_\psi^d = M_\psi R_d/\tau_\psi, \tag{8}$$

if there is to be suppression. The lower of the two limits (7) and (8) on the transverse momentum thus determines up to where there will be a reduction of the signal.

We should note here that the spatial restriction (8) depends only on the size of the matter bubble, and on the parameters of the $\psi(M_\psi, \tau_\psi)$; it does not depend on the density of the medium. In contrast, the temporal condition (5) contains the time t_ψ^d at which the medium has become too cold to suppress, and the greater the density of the medium is, the longer it will take to reach that point, i.e. the bigger t_ψ^d will be. As a consequence, the temporal restriction tends to be the relevant one for systems which are large and/or of relatively low density. The spatial size of the medium, on the other hand, becomes decisive for the P_T limit of suppression for small and/or very dense bubbles. We shall shortly make these statements more quantitative.

We have so far considered the ψ; analogous restrictions can be obtained for the other heavy quark bound states. However, relations (7) and (8) contain the masses M_x and the formation times τ_x, which are different for the different bound states x. Hence the restrictions due to finite size and life-time of the medium depend on the bound state in question. As just noted, the dissociation time limit t_x^d in addition depends on the initial density of the medium. We thus have relations for the suppression of heavy quark bound states depending on what state we consider, on its transverse momentum, and on the initial density of the suppressing environment. This gives us the basis for our spectral analysis.

Before we consider nuclear collisions with realistic geometric features, we want to illustrate the essential features of the analysis in somewhat simplified situations.

3 Suppression in idealized systems

3.1 Colour screening in an infinite system

If our deconfining systems were so large that we could safely neglect any restrictions from the spatial extension of the plasma, then (7) would restrict the suppression range. It turns out that in general (7) is indeed the relevant restriction, but more because the initial density is relatively low and hence the plasma life-time rather short. Nevertheless, this means that the simplified case we treat here does form the basis of later and more realistic considerations.

To determine the limiting time t_x^d, up to which the system dissociates a given heavy quark bound state x, we need to know up to what temperature this state can remain bound. This question was partially answered in [28], where the values of the screening mass μ_x (the inverse of the colour screening length) necessary for the dissociation of the different states x were calculated; the resulting values are listed in Table 1. The temperature dependence of the screening mass in the quark-gluon plasma is the subject of extensive studies in lattice QCD. Although a final answer cannot yet be given, the results obtained up to now [35] are reasonably well parametrised by

$$\mu(T)/T_c = 4(T/T_c), \tag{9}$$

where $T_c \simeq 150$ MeV is the critical temperature for deconfinement and chiral symmetry restoration. The temperatures $T_x^d \equiv c_x T_c$, with $c_x \geqq 1$, necessary for the dissociation of the different states x, are also shown in Table 1; they follow from (9) and the listed values of μ_x. What we now still have to know is the rate of cooling of the system: given some initial temperature T_o, how quickly will a plasma of this temperature expand and cool down to some particular value T_x^d? For longitudinal isentropic expansion, times and entropy densities are related by

$$s(t_o)\, t_o = s(t_x^d)\, t_x^d, \tag{10}$$

where t_o denotes the time necessary to create the plasma; we shall take $t_o = 1$ fm, as is generally assumed. For an ideal gas, the entropy density s is proportional to T^3; using this, we get

$$P_x^d = M_x \left[\left(\frac{t_o}{\tau_x} \left[\frac{T_o}{T_x^d} \right]^3 \right)^2 - 1 \right]^{1/2} = M_x \left[\left(\frac{t_o}{\tau_x} \left[\frac{T_o}{c_x T_c} \right]^3 \right)^2 - 1 \right]^{1/2} \tag{11}$$

as the limiting transverse momentum for the suppression of a heavy quark bound state x; for P_T^x above this value, there is no more suppression of state x.

Since the initial temperature is less easily estimated than the energy density, we use the Stefan-Boltzmann relation for an ideal quark-gluon plasma to rewrite (11) in the form

$$P_x^d = M_x \left[\left(\frac{t_o}{c_x^3 \tau_x} \left[\frac{\varepsilon}{\varepsilon_c} \right]^{3/4} \right)^2 - 1 \right]^{1/2}, \tag{12}$$

where ε is the initial value of the energy density, and ε_c its value at the critical temperature T_c. Using (12) with the parameters listed in Table 1, we now calculate the transverse momentum limit on the suppression of heavy quark bound states, P_x^d, for the different $c\bar{c}$ and $b\bar{b}$ resonances. The result is shown in Fig. 1a. The limiting curve for the Υ is not included here, because Υ suppression does not start until $T_o/T_c \simeq 2.6$, which implies $\varepsilon/\varepsilon_c \gtrsim 50$ – a range not soon expected to be attainable in heavy ion collisions.

For an infinite plasma, there is complete suppression of bound state x for all transverse momenta less than P_x^d, and no suppression beyond that point. This is clearly a rather crude picture and will be refined by geometric considerations in Sect. 4. Nevertheless, we can use it here to obtain some idea on the overall suppression for the different states. The production rate of the different resonances decreases quite steeply with P_T; for P_T not too large, we can take it to be approximately exponential in the transverse mass $(P_T^2 + M^2)^{1/2}$. The survival probability $S_x(\varepsilon)$ for the state x is thus essentially given by

$$S_x(\varepsilon) \simeq \exp\{-\lambda\{[(P_d^x)^2 + M_x^2]^{1/2} - M_x\}\}. \tag{13}$$

For the $c\bar{c}$ states, the canonical hadronic value $\lambda \simeq 6\ \mathrm{GeV}^{-1}$ gives reasonable agreement with the measured P_T distribution. Using this, we get patterns shown in Fig. 2a; for the $b\bar{b}$ states, they should be considered just as an illustration, since the validity of (13) with the hadronic value of λ is certainly questionable. But in any case we here only want to illustrate how such patterns can be obtained; for a realistic estimate, further features and details of the collision geometry and of the P_T distributions of the charmonium/bottonium states have to be

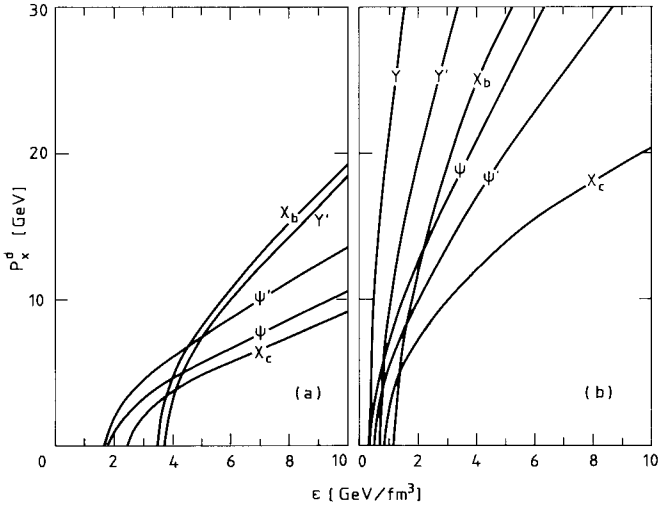

Fig. 1a, b. Transverse momentum limits for suppression by colour screening **a** and by absorption **b**

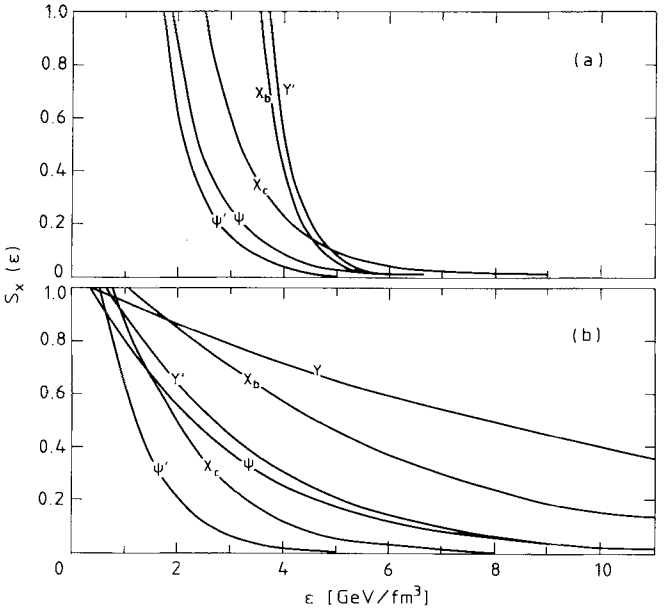

Fig. 2a, b. The energy density dependence of suppression by colour screening **a** and by absorption **b**

included. Moreover, the abruptness of the suppression onset is further softened also by a quantum-mechanical treatment of the formation time [29–31], as already mentioned.

For colour screening, the initial energy density or temperature of the medium are the natural variables. Experimentally, however, one generally obtains the final density of the secondaries and their energies, rather than ε or T. It is therefore necessary to relate ε to the experimentally measured quantities. One proposal [36], based on freely expanding secondaries, gives for the initial energy density

$$\varepsilon = (\mathrm{d}N/\mathrm{d}y)\,\bar{p}_o/(S_{\mathrm{eff}}\,t_o), \tag{14}$$

where $\mathrm{d}N/\mathrm{d}y$ is the number of observed secondaries per unit rapidity interval, $\bar{p}_o$ the average energy per secondary, and S_{eff} the effective overlap area in the collision. On the other hand, assuming isentropic longitudinal expansion [37] instead of free flow leads to

$$s_o = 3.6(\mathrm{d}N/\mathrm{d}y)/(S_{\mathrm{eff}}\,t_o) \tag{15}$$

for the initial entropy density. For an ideal gas of gluons and three flavours of massless quarks, energy density and entropy density are given by $\varepsilon = (47.5\pi^2/30)\,T^4$ and $s = (63.3\pi^2/30)\,T^3$, respectively. Using these relations together with (15), we get

$$\varepsilon = 1.5[(\mathrm{d}N/\mathrm{d}y)/(S_{\mathrm{eff}}\,t_o)]^{4/3} \tag{16}$$

for the initial energy density in the case of hydrodynamic expansion along the beam axis. Although the latter thus gives for very high multiplicities a higher initial energy density than obtained from free flow, the two forms differ rather little (less than 20%) in the energy range from SPS to LHC [38, 39]. Since we have assumed longitudinal hydrodynamic expansion in determining the transverse momentum limit (11), we shall for consistency in the following use (16) for the initial energy density.

3.2 Absorption in an infinite system

Let us now see what form of suppression arises in an infinitely large, expanding medium due to absorption. The survival probability for a heavy quark bound state x in a medium of density $n(t)$ is given by

$$S_x(t_f) = \exp\left\{-\int_{t_x}^{t_f} \mathrm{d}t\, n(t)\,\sigma_x\right\}. \tag{17}$$

Here t_f is the time at which the medium has become too dilute to be considered an interacting hadron gas; since this is just the freeze-out time, when strong interactions stop, it does not depend on the bound state x in question. In contrast, we had in the deconfinement approach as corresponding quantity the time t_x^d, up to which the medium could melt the bound state x, and t_x^d does depend on what bound state we are considering. As in Sect. 3.1, we denote by t_x the formation time for the bound state x in the rest-system of the absorbing medium. We assume t_x to be at least as long as the thermalisation time t_o, the time after which the interacting environment can be considered a hadron gas, i.e., a thermal system. When this is not the case (we shall take $t_o = 1$ fm, and from Table 1 we see that ψ and Υ formation times are slightly shorter), we replace t_x by t_o in (17). We shall also consider the simplest version of absorption and assume the break-up cross section σ_x to be time-independent. The density $n(t)$ of the absorbing medium is obtained by tracing back the observed hadronic secondaries in the final state to the interaction volume at the initial thermalisation time t_o; this time is in the absorption picture the counterpart to the plasma formation time t_o in Sect. 3.1. We thus set

$$n(t_o) = (\mathrm{d}N/\mathrm{d}y)/(z_o\,S_{\mathrm{eff}}), \tag{18}$$

where $\mathrm{d}N/\mathrm{d}y$ is the multiplicity per unit central rapidity interval, S_{eff} the transverse size of the medium at the time of its formation, and z_o the corresponding longitudinal extension. Assuming again isentropic longitudinal expansion, we get

$$n(t) = (t_0/t)\,n_0 = (\mathrm{d}N/\mathrm{d}y)/(tS_{\mathrm{eff}}), \tag{19}$$

where we have defined $n_o \equiv n(t_o)$ and set $z_o = t_o = 1$ fm. Carrying out the integration in (17), we get

$$S_x(t_f) = (t_x/t_f)^{\kappa_x}, \tag{20}$$

with

$$\kappa_x \equiv n_o\,t_o\,\sigma_x = \sigma_x(\mathrm{d}N/\mathrm{d}y)/S_{\mathrm{eff}}. \tag{21}$$

The validity of assuming longitudinal expansion only is much more questionable here than for a plasma with its much shorter life-time. If we assume three-dimension-

al isentropic expansion, then (19) is replaced by

$$t/t_o = [n(t_o)/n(t)]^{1/3}, \tag{22}$$

and the resulting freeze-out time is much shorter. As a consequence, there remains a considerable uncertainty in the value of the freeze-out density as well. Following the estimates of [16] (where a realistic three-dimensional expansion was considered), we shall use the freeze-out density $n_f \equiv n(t_f) = 1.0\ \mathrm{fm}^{-3}$ and retain an effective longitudinal expansion of the form (19). Note that with (15) and (16), this value of n_f gives at freeze-out an energy density of about 0.3 GeV/fm^3, i.e., about a third of that needed for deconfinement.

For bound states at rest in the medium, $t_x = \tau_x$, and the formation times τ_x are listed in Table 1. It remains to determine the other crucial quantity distinguishing the different bound states, the break-up cross sections σ_x. The only heavy quark bound state for which there seem to exist cross section data is the ψ; one finds [40] $\sigma_\psi \simeq 1$–3 mb for the total $\psi - p$ cross section. To obtain the corresponding values for the other states, we take recourse to geometric arguments [41], which lead to the relation

$$\sigma_x/\sigma_y = r_x^2/r_y^2, \tag{23}$$

for the ratio of the cross section of a hadron x incident on a proton target to that of another hadron y on a proton target. Here r_x^2 denotes the mean square radius of hadron x. In Table 1, we have listed the values [28] of r_x as well as the cross sections obtained with $\sigma_\psi = 1$ mb as input, assuming half the total cross section to be due to break-up reactions.

Using (19), we obtain for the suppression function (20) the form

$$S_x(n_o) = [(t_x/t_o)(n_f/n_o)]^{n_o t_o \sigma_x}, \tag{24}$$

expressed in terms of the initial hadron density n_o, which is related to the observed secondary multiplicity $\mathrm{d}N/\mathrm{d}y$ by (18), and the freeze-out density n_f. To compare this form of suppression to that obtained in the colour screening approach, we express the energy density used as variable in Sect. 3.1 in terms of $\mathrm{d}N/\mathrm{d}y$ through (13) or (14). In Fig. 2b, we show the variation of the absorption for the different bound states as function of ε. The corresponding behaviour in the colour screening approach was shown in Fig. 2a, where we can set $\varepsilon_c = 1$ GeV/fm^3 (corresponding to $T_c = 150$ MeV) to get a direct comparison. We note in particular that absorption provides a much more gradual suppression than deconfinement, and that the break-up of the Υ begins much earlier than its dissolution by colour screening.

The momentum limit of suppression due to absorption is functionally the same as in the deconfinement picture: if the $c\bar{c}$ or $b\bar{b}$ state has a sufficiently high momentum, it will not yet have formed a "full-sized" resonance when the medium has become too dilute to break it up. Hence the end of suppression is again given by (7), but now with the universal freeze-out time t_f in place of t_x^d. Using relation (19), we thus obtain

$$P_x^d = M_x[(t_o/\tau_x)^2 (n_o/n_f)^2 - 1]^{1/2} \tag{25}$$

for the momentum limits of absorption. These limits are shown in Fig. 1b, to be compared to the deconfinement limits of Fig. 1a. We note in particular that in the energy density range of interest, i.e., $\varepsilon \geqq 2$ GeV/fm^3, there is absorption up to much higher momenta than there was suppression by colour screening. For example, at $\varepsilon = 3$ GeV/fm^3, suppression by deconfinement stops at $P_T = 2$–4 GeV for the $c\bar{c}$ states, while absorption stops only at $P_T = 10$–15 GeV. The reason for this difference is, of course, that at $\varepsilon = 3$ GeV/fm^3, deconfinement stops for the ψ at $t_\psi^d \simeq 1.4$ fm, while absorption continues until more than twice this value. As a consequence, the restriction due to the finite life-time of the absorbing medium thus does not prove to be very stringent for transverse momenta below 10 GeV.

3.3 Suppression due to finite spatial extension

To test the role of spatial restrictions on the suppression of heavy quark bound states, we now consider the case in which (8) provides the relevant limit; this would be the case for a medium of very high density or small spatial extension. The former is difficult to achieve in heavy ion collisions. However, for lighter projectiles or not very central collisions, the volume of the hot matter bubble can be so small that (8) in fact does become the crucial condition.

As we had seen, (8) gives us the momentum for which the $c\bar{c}$ or $b\bar{b}$ state can escape unaffected from the region of suppression, for deconfinement as well as for absorption. If we assume for the moment a uniform distribution in energy density (we will come to a more realistic picture in Sect. 4), then for fully central collisions, i.e., at impact parameter $b = 0$, the radius of the bubble R_d and the radius of the projectile nucleus R_A coincide. On the average, a $c\bar{c}$ or $b\bar{b}$ pair then has to traverse a distance R_A of dense matter. This gives us the limiting transverse momenta for suppression, shown in Table 2 for Pb–Pb collisions; they are to be compared to the limits from finite life-time restrictions shown in Fig. 1.

In the deconfinement approach, we conclude that the short plasma life-time gives the more important limit up to very high energy densities; only for $\varepsilon/\varepsilon_c \geqq 15$ GeV/fm^3 do the spatial restrictions begin to dominate the temporal. Thus in the density range we expect to attain, the plasma temperature has in general fallen below the hadronisation point much before an average $c\bar{c}$ or $b\bar{b}$ pair has a chance to leave the spatial region of the medium. The effective overlap area decreases, how-

Table 2. Spatial limits P_x^d [GeV] of suppression for a system of infinite life-time (Pb–Pb collisions)

States	ψ	ψ'	χ_c	Υ	Υ'	χ_b
P_x^d	22	17	12	68	37	27

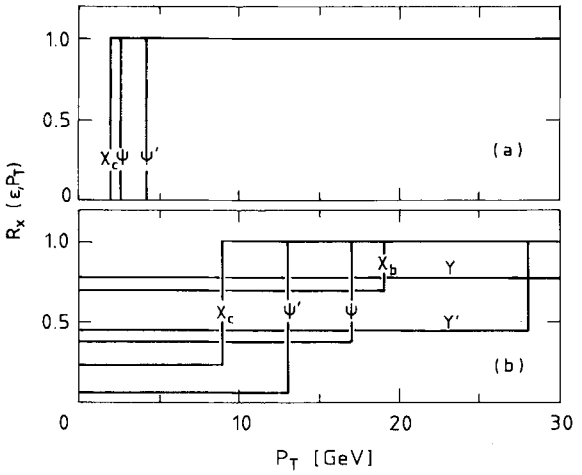

Fig. 3a, b. The transverse momentum dependence of suppression by colour screening **a** and by absorption **b**, for $\varepsilon = 3$ GeV/fm^3

ever, as the collision becomes less central; this, as well as bound state production at the edges of the deconfining region, requires both temporal and spatial restrictions to be included in a realistic description of a nuclear collision, particularly at very high energies.

In the absorption picture, the longer life-time of the medium makes the spatial restriction more important. Comparing the values in Fig. 1 with those in Table 2, we see that for central Pb−Pb collisions, the transition from temporal to spatial suppression limit occurs at $\varepsilon \simeq 4$ GeV/fm^3. Assuming as in Sect. 3.1 that the P_T distribution of the $c\bar{c}$ and $b\bar{b}$ states falls rapidly with increasing P_T, we can nevertheless retain Fig. 3 as a good approximation for the integrated suppression behaviour.

It should be noted, however, that in the absorption picture neither of the two limits provides an end to suppression anywhere near where it is found experimentally [7–11], i.e., around 2–3 GeV. In the range of momenta so far covered by experiments, absorption alone does not give the observed momentum dependence of the suppression [12–17]; in fact, if the absorbing medium were pion gas, the absorption would even increase with increasing P_T, because of the break-up threshold due to the mass difference between the J/ψ and a $D\bar{D}$ pair. To arrive at a viable description of the data, absorption as origin of the suppression is combined with initial state parton scattering [42, 43] to shift $c\bar{c}$ (or $b\bar{b}$) production to higher P_T [18–20]. We shall return to this point shortly.

3.4 Suppression patterns in P_T

In Fig. 2 we had already seen that in comparison to colour screening, absorption leads to a more gradual onset of suppression in general, and to an earlier Υ suppression in particular. For the simplified world which we are considering here, let us now illustrate the effects that the finite life-time or the finite size of the medium have on the P_T dependence of the suppression in the different approaches. We consider the survival probability at fixed ε and P_T,

$$R_x(\varepsilon, P_T) = \frac{(\mathrm{d}\sigma_x(\varepsilon, P_T)/\mathrm{d}P_T^2\, \mathrm{d}y)_{y=0}}{(\mathrm{d}\sigma_x(0, P_T)/\mathrm{d}P_T^2\, \mathrm{d}y)_{y=0}}, \tag{26}$$

where the numerator describes the production of a system x in a medium of initial energy density ε and the denominator that for some $\varepsilon \leqq \varepsilon_c$, e.g., for $\varepsilon \to 0$. Neglecting surface effects, we get from colour screening a complete suppression for $P_T \leqq P_x^d$, with P_x^d in general determined by the plasma life-time. This leads to a number of "deconfinement" thresholds, as shown in Fig. 3a.

In the absorption approach, suppression occurs up to much higher values of P_T, and for a system of finite size, there is only partial suppression even when $P_T \leqq P_x^d$. Taking the suppression for the different states to be essentially P_T-independent for $P_T^x \leqq P_x^d$ ⋆, we can write

$$\mathrm{d}\sigma_x(\varepsilon, P_T)/\mathrm{d}P_T^2 \simeq \sigma_x(\varepsilon)\, \Theta(P_T - P_x^d) \tag{27}$$

to obtain

$$R_x(\varepsilon, P_T) \simeq \frac{\sigma_x(\varepsilon)}{\sigma_x(0)}\, \Theta(P_T - P_x^d) = S_x(\varepsilon)\, \Theta(P_T - P_x^d), \tag{28}$$

neglecting the small contributions to the cross-section from to $P_T > P_d^x$. The result is shown in Fig. 3b.

The effects of deconfinement and absorption differ in particular for high energy densities or small volumes. In the deconfinement approach, the short plasma life-time provides the crucial restriction, and hence the endpoint of suppression moves with increasing ε to higher P_T. In contrast, the endpoint of suppression in the absorption picture is determined by the size of the bubble already for rather low values of ε (for $\varepsilon \geqq 4$ GeV/fm^3 in case of central Pb−Pb collisions); from then on, it is independent of ε. For states with $P_T \simeq 0$, the life-time of the medium provides the decisive restriction in both cases.

Finally, let us see what initial state parton scattering does to the absorption patterns. It is now assumed that the partons which eventually interact to form the $c\bar{c}$ or $b\bar{b}$ pair undergo multiple elastic scattering in the nuclear medium *before* this interaction [42–44]. This shifts the final parton-parton interaction axis relative to the beam axis. It therefore adds an initial state contribution Δ_x to the mean squared transverse momentum of the bound state x, if that state is produced in a nuclear environment:

$$\langle P_T^2 \rangle_x - \langle P_T^2 \rangle_{ox} = \Delta_x. \tag{29}$$

Here $\langle P_T^2 \rangle_{ox}$ denotes the mean squared P_T of the bound state x produced in a $p-p$ collision. The initial state contribution Δ_x depends on the density of the environment, and hence through the number of participants, N_{AB}, on the transverse hadronic energy E_T. For higher E_T, there are more participants and thus more possible initial state scatterings. For a given parton-parton inter-

⋆ We assume that resonance contributions compensate the mentioned increase of suppression with P_T; see [14, 15]

action (e.g., gluon fusion), Δ_x depends on N_{AB}, but not on which final state is produced, and thus all $c\bar{c}$ and $b\bar{b}$ pairs formed in such an interaction will receive the same initial "kick". At fixed $\sqrt{s}$, this gives to all heavy quark states as well as to Drell-Yan production [45] the same functional dependence of the P_T broadening Δ_x on E_T

$$\Delta_x(E_T) = c_x f_{AB}(E_T). \tag{30}$$

As a consequence, the ratio of the P_T-broadening for two different states x and y, $\Delta_x/\Delta_y = c_x/c_y$, becomes independent of E_T and hence of ε. This is in contrast to the ε-dependent patterns which arise from the different $P_x^d(\varepsilon)$ in the deconfinement picture. We should also note at this point that for colour screening, the P_T-behaviour of charmonium and bottonium suppression depends on ε, while initial state parton scattering results in a dependence on the number of participants or, equivalently, on E_T. If we can vary E_T without changing ε, then the two descriptions will lead to different patterns.

If we parametrise the P_T-dependence of the production cross-sections in an exponential form,

$$\mathrm{d}\sigma_x/\mathrm{d}P_T^2 = \sigma_x \left\{\frac{2}{\langle P_T\rangle_x}\right\}^2 \exp\left\{\frac{-2P_T}{\langle P_T\rangle_x}\right\}, \tag{31}$$

then for production in a collision leading to a transverse energy E_T, the mean P_T in (31) (with $\langle P_T^2\rangle_x = (3/2)\langle P_T\rangle_x^2$) is determined through (29), i.e., it depends on E_T through Δ_x. Using (31), we find that the essentially P_T-independent suppression rate $R_x(\varepsilon, P_T) \simeq S_x(\varepsilon)\,\Theta(P_T - P_x^d)$ now is multiplied by the factor

$$F_x(P_T) = \left\{\frac{2}{\langle P_T\rangle_x}\right\}^2 \exp\left\{\frac{-2P_T}{\langle P_T\rangle_x}\right\}, \tag{32}$$

giving us for $P_T < P_x^d$

$$\tilde{R}_x(\varepsilon, P_T) = S_x(\varepsilon)\left\{\frac{\langle P_T\rangle_{ox}}{\langle P_T\rangle_x}\right\}^2 \exp\left\{\frac{2P_T}{\langle P_T\rangle_{ox}}\left[1 - \frac{\langle P_T\rangle_{ox}}{\langle P_T\rangle_x}\right]\right\}. \tag{33}$$

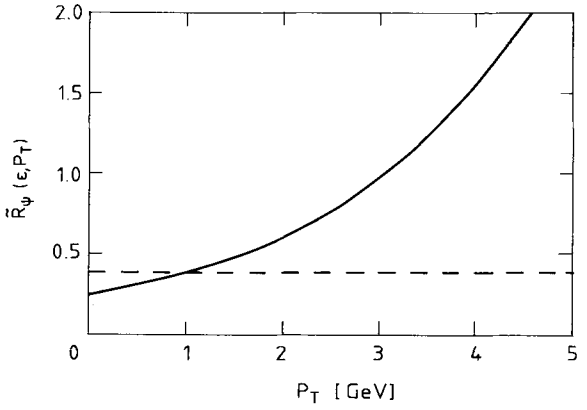

Fig. 4. The transverse momentum dependence of ψ suppression by absorption with (solid line) and without (dashed line) initial state scattering, for $\varepsilon = 3$ GeV/fm^3

The resulting behaviour is schematically illustrated in Fig. 4 for the ψ, using numerical values for Δ_x corresponding to data from $p-p$ and O–U collisions at $\sqrt{s} = 20$ GeV [11, 40]. We note that although the introduction of a momentum dependence in this form does not change the integrated suppression rate, it still leads to more suppression at small P_T, paid for by an enhancement at large P_T.

The situations we have considered in this section – a uniform suppressing medium of either large size or long life-time – are clearly very much oversimplified. In the next section, we shall therefore adopt a more realistic picture of nuclear collisions.

4 Conditions in nucleus-nucleus collisions

4.1 The geometry of nuclear collisions

The dense multi-particle systems formed in nuclear collisions are created in a small region of space-time. The major consequences of this for the suppression pattern of heavy quark resonances have been discussed in the previous sections for systems of uniform density. In the cms-frame of an actual high energy nucleus-nucleus ($A-B$) collision, however, the nuclei are Lorentz-contracted disks of 1 fm thickness and transverse radius $R_A = 1.2A^{1/3}$. For the radial distribution of the nucleon number in such a Lorentz-contracted nucleus one obtains

$$\mathrm{d}A/\mathrm{d}r^2 \equiv n_A(\mathbf{r}) = 2R_A\rho_A\left(1 - \left(\frac{r}{R_A}\right)^2\right)^{1/2}, \tag{34}$$

where $\mathbf{r}$ denotes a two-component vector in the transverse plane and $\rho_A = 3A/4\pi R_A^3$ the uniform distribution of nucleons in a nucleus at rest. As a result, the density in a central collision of two equal nuclei will be highest in the center and fall off toward the edges of the interaction region.

In a non-central $A-B$ collision, the two nuclei may overlap only partly. Nucleon-nucleon interactions then occur only in the overlap region of the nuclei, so that the total transverse energy E_T measured in such collisions is initially concentrated in this interaction volume. It decreases with increasing impact parameter b because the transverse overlap area S_{eff} as well as the nucleon number density decrease. The functional form of the b-dependence of E_T, however, as well as its dependence on A and B, are theoretically not uniquely determined. In particular, there are different forms which relate E_T either to the average number of participants or to the average number of nucleon-nucleon collisions at given impact parameter. The existing data for O–U and S–U collisions [46], however, seem to be consistent with the assumption that the total E_T produced in these collisions is proportional to the number of participants. We therefore use this parametrization in the following discussion of the E_T dependence of the suppression pattern.

For a collision at impact parameter b, the number of participants is given by

$$N_{AB}(b) = \int_{S_{\text{eff}}} d^2 r (n_A(\mathbf{r}) + n_B(\mathbf{r}-\mathbf{b})). \tag{35}$$

The corresponding energy density in the interaction volume $S_{\text{eff}}(b)\, z_o$ thus becomes (see (16))

$$\varepsilon(b) = 1.5 \left[N_{AB}(b) \left\{ \frac{(dN/dy)_o}{2(S_{\text{eff}}(b)\, z_o)} \right\} \right]^{4/3}, \tag{36}$$

where $(dN/dy)_o$ is the average number of secondaries in a $p-p$ collision; we shall take the longitudinal dimension z_o of the interaction region at the initial time $t_o \simeq 1$ fm to be also of the order of a fermi. In a central $A-B$ collision the number of participants is given by

$$N_{AB}(0) = \begin{cases} 2A & \text{for } A = B, \\ 1.5\, A^{2/3} B^{1/3} + A & \text{for } A \ll B. \end{cases} \tag{37}$$

At fixed cms-energy, the resulting gain in energy density in going from O–Pb to Pb–Pb collisions becomes less than 10%. This, however, may be too conservative an estimate; in fact, in the standard Glauber model description of nucleus-nucleus collisions, the mean transverse energy is expected to increase as $AB^{1/3}$ in an average $A-B$ collision [47].

The behaviour of the average energy density $\varepsilon(b)$ in the overlap region S_{eff} as function of the transverse energy fraction $E_T(b)/E_T(0)$ is shown in Fig. 5, for the cases $A \ll B$ and $A = B$. We note that in an asymmetric collision the energy density decreases by about 50% as we go from $E_T(b)/E_T(0) = 1.0$ to 0.3, whereas for symmetric collisions it remains essentially constant over this range. In the latter case the decrease in $N_{AB}(b)$ with increasing impact parameter is accompanied by a corresponding decrease of S_{eff}; thus the two effects tend to compensate and lead to a nearly constant energy density. In asymmetric collisions ($A < B$), on the other hand, a big decrease in ε occurs in the region where the smaller nucleus still is completely immersed in the larger one; here N_{AB} varies with b, while S_{eff} remains constant. In the case of a very large asymmetry (for $B \to \infty$ at fixed A), $\varepsilon(b)$ varies with the transverse energy as $(E_T(b))^{4/3}$, as expected from (37) and the linear relation between E_T and the number of participants. The deviation from this behaviour seen in Fig. 5 at small E_T reflects the more rapid drop in the number of participants when the two nuclei overlap only in part. It depends sensitively on the specific geometric "edges" of the nuclei and hence is more a surface than a volume effect. Therefore this region is not well suited to study variations in energy density.

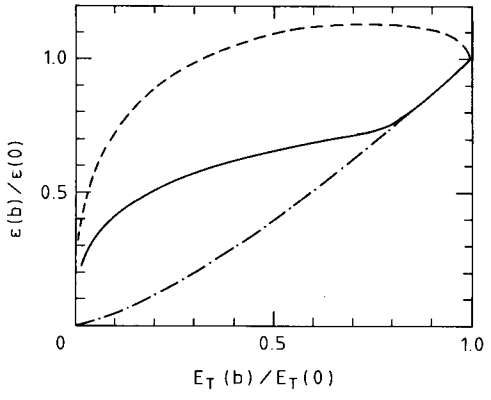

Fig. 5. The dependence of the energy density on the transverse energy for $A-A$ (dashed line) and $A-B$ collisions, with $A \gg B$ (dash-dotted line). The solid line shows the form for S–Pb collisions

From Fig. 5 we conclude that in $A-A$ collisions a variation of E_T over a large range does not lead to much change in the energy density ε. As noted above in Sect. 3.4, this can in principle be used to distinguish between deconfinement and initial state parton scattering as mechanisms for the P_T-dependence of suppression. While the latter leads to less broadening for smaller E_T, the former depends only on ε.

Due to the inhomogeneous nuclear density distribution (35), the energy density distribution in the overlap region $S_{\text{eff}}(b)$ is also not constant,

$$\varepsilon(b, \mathbf{r}) \sim \{n_A(\mathbf{r}) + n_B(\mathbf{r}-\mathbf{b})\}^{4/3}. \tag{38}$$

In Fig. 6 we show the energy density profile in central $A-B$ collisions for $A \ll B$ and $A = B$. One thus finds that for a central $A-A$ collision the energy density in the center is about 50% higher than the average energy density. It is this effect, as we shall see, that makes Pb–Pb collisions much more effective for the suppression of $c\bar{c}$ and $b\bar{b}$ bound states than S–Pb collisions at the same energy, even though the average energy density in the two cases differs only rather little, as we had seen. Figure 6 is easily translated into a temperature profile for

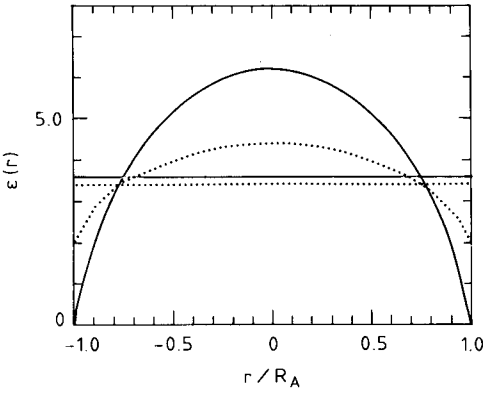

Fig. 6. The energy density profile for central $A-A$ (solid line) and $A-B$ (dotted line) collisions; the straight lines give the average values in each case

* We could also use the energy density profile shown in Fig. 6 and combine it with an equation of state that incorporates a (first order) phase transition, to derive the corresponding temperature profile. This would then give a region with constant temperature close to the boundaries of S_{eff}, as reflection of the first order transition [4]. We will, however, discuss here only suppression by screening in a quark-gluon plasma or by absorption in a dense hadron gas, so that a two-phase equation of state is not needed

an ideal quark-gluon plasma ($\varepsilon \simeq 15.6\,T^4$) or an ideal pion gas ($\varepsilon \simeq T^4$).

In order to discuss the suppression of heavy quark resonances, we also have to specify the spatial distribution of the heavy quark-antiquark pairs created initially in a hard collision. We assume this distribution to be proportional to the total number of collisions, so that

$$n_{Q\bar{Q}}(\mathbf{r}) \sim n_A(\mathbf{r})\, n_B(\mathbf{r}-\mathbf{b}). \tag{39}$$

gives the pair production density $n_{Q\bar{Q}}$, where Q denotes either c or b.

4.2 The energy dependence of the input parameters

We want to study in the following the suppression patterns for different cms energies of the incident nuclei; of particular interest are the energy of the SPS at CERN and the energies planned for RHIC at BNL and for the LHC at CERN. The dependence on the cms energy enters our calculations in two places. It is necessary for estimating the initially created energy density, and it determines the form of the P_T-distribution for the production of $c\bar{c}$ and $b\bar{b}$ pairs.

In a $p-p$ collision at $\sqrt{s}=20$ GeV, the total number of secondaries (charged plus neutral) is found to be $(\mathrm{d}N/\mathrm{d}y)_o \simeq 2.4$, with an average m_T of about 0.5 GeV. Recent results from S–S collisions at the SPS [48] indicate that the average number of secondaries per participant is somewhat higher, with $(\mathrm{d}N/\mathrm{d}y)_{SS}/32 \simeq 3$ [49]; this indicates that rescattering effects may become important in nucleus-nucleus collisions. We will therefore use the multiplicity form

$$(\mathrm{d}N/\mathrm{d}y)_o = c \ln \sqrt{s}, \tag{40}$$

with $c=1$ instead of the value $c=0.8$ obtained for $p-p$ collisions [50], to determine the energy densities (37). The average energy densities in S–S, S–Pb and Pb–Pb collisions thus obtained for the SPS ($\sqrt{s}=20$ GeV), for RHIC ($\sqrt{s}=200$ GeV), and for the LHC ($\sqrt{s}=6300$ GeV) are summarized in Table 3. These numbers will be used as the input for the numerical analysis of the suppression patterns to be presented in the next section.

The P_T dependence of dilepton production has been studied extensively for $p-p$ collisions [51]. The general form of the mean P_T as given by QCD is [52]

$$\langle P_T \rangle_o = a + \sqrt{s}\, f(\tau), \tag{41}$$

Table 3. Expected average energy densities [GeV/fm^3] for central S–S, S–Pb and Pb–Pb collisions at SPS, RHIC and LHC energies

	S–S	S–Pb	Pb–Pb
SPS (20 GeV)	0.80	1.75	1.82
RHIC (200 GeV)	1.71	3.75	3.90
LHC (6.3 TeV)	3.34	7.32	7.62

where a denotes the contribution from the intrinsic Fermi motion of the incident partons in the nucleon; the second term, with $\tau \equiv M^2/s$, contains soft gluon emission of the incident parton as well as hard scattering contributions (e.g., from quark-gluon Compton scattering). The linear rise of $\langle P_T \rangle_o$ with $\sqrt{s}$ at fixed τ is empirically confirmed. At fixed s, $f(M^2/s)$ does not seem to vary strongly with M; in particular, it appears to become rather constant for $\sqrt{\tau} \geqq 0.2$ [53]. Since we want to consider here the dilepton mass range $3\ \mathrm{GeV} \leqq M \leqq 10\ \mathrm{GeV}$ as $\sqrt{s}$ grows from 20 to 6300 GeV, we need to know the behaviour of $f(\tau)$ in the limit of small τ, which is not very well established. To get a first idea of what behaviour we should expect, we will use the exponential P_T behaviour (31) with the parametrisation

$$\langle P_T \rangle = 0.3 - 10^{-1} \sqrt{s}\,(\sqrt{\tau} \ln \sqrt{\tau}). \tag{42}$$

This form is in accord with all existing data for Drell-Yan production in pp and $p\bar{p}$ collisions up to $\sqrt{s}=62$ GeV, as well as with results for Drell-Yan production in terms of the leading QCD contributions [54]. For charmonium production, there is a higher intrinsic P_T; the constant term is here about twice the value given in (42). For the average P_T of the ψ, (42) leads to an increase by a factor two to three between SPS and LHC energies.

To include initial state parton scattering in the absorption picture, we must also fix the dependence of the P_T-broadening on the initial state parameters. For this, we take the form introduced in [19, 55], which for central collisions becomes

$$(\Delta P_T^2)_{AB} \simeq \langle P_T^2 \rangle_{gN}\, \sigma_{gN}\, n_s\, 0.9 (A^{1/3} + B^{1/3}); \tag{43}$$

as already mentioned above, it relates the P_T broadening in nuclear matter to the number of elastic interactions between the incoming gluon and the target nucleons, before the gluon fuses with another gluon to form the observed $c\bar{c}$ state. In (43), σ_{gN} denotes the elastic gluon-nucleon cross-section. The remaining factor, with n_s denoting standard nuclear density, describes the average thickness of the matter traversed. The average P_T^2 in a gluon-nucleon interaction can be determined from J/ψ production in $p-p$ collisions, the cross-section $\sigma_{gN} \langle P_T^2 \rangle_{gN}$ from a comparison of J/ψ production in $p-p$ and $p-A$ collisions [19]. This leads to

$$(\Delta P_T^2)_{AB} / \langle P_T^2 \rangle_o \simeq 0.03 (A^{1/3} + B^{1/3}); \tag{44}$$

and forms the input for the initial state scattering results shown in the next section. Note, however, that it is based on ψ production by gluon fusion; an increased contribution from quark-gluon interactions would presumably reduce the quoted value, since the P_T broadening in Drell-Yan production is only half that found for the J/ψ. For the other $c\bar{c}$ and for the $b\bar{b}$ bound states, we have the same uncertainty. To obtain definite predictions, we shall simply use (44), keeping in mind this caveat.

5 Patterns of charmonium and bottonium production in nuclear collisions

With the nuclear geometry and the input parameters fixed, we now want to look at the spectral patterns as predicted for specific experiments. We begin with J/ψ production at the SPS for S–S, S–Pb and Pb–Pb collisions, followed by the expected ratios of ψ' to J/ψ production. Next we shall compare ψ production at SPS, RHIC and LHC energies, and finally we shall compare the fate of ψ and Υ in Pb–Pb collisions at both RHIC and LHC energies.

Let us first look how in the different models the suppression of the J/ψ depends on target and projectile at SPS energy. Note that here we will consider the actually observed J/ψ, i.e., a superposition of 60% direct ψ production and 40% from χ_c decay. In Fig. 7, we show the P_T dependence of the suppression; in Fig. 7b, showing the case for S–Pb collisions, we have included the S–U data from [11]. In Fig. 8, we consider the corresponding E_T dependence, again with the data [11] for the S–U case.

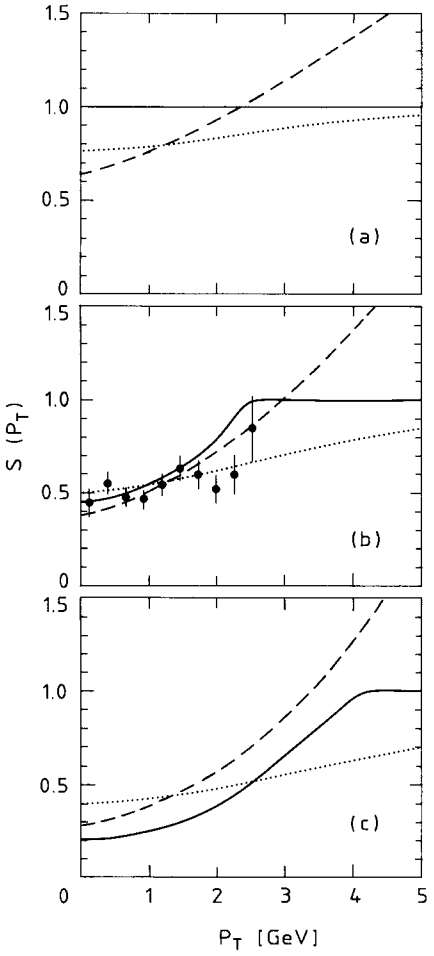

Fig. 7a, b. The P_T dependence of J/ψ suppression for S–S **a**, S–Pb **b** and Pb–Pb collisions at the SPS. Shown are the predictions from colour screening (solid line), absorption (dotted line) and absorption with initial state scattering (dashed line); the data in **b** are from [11]

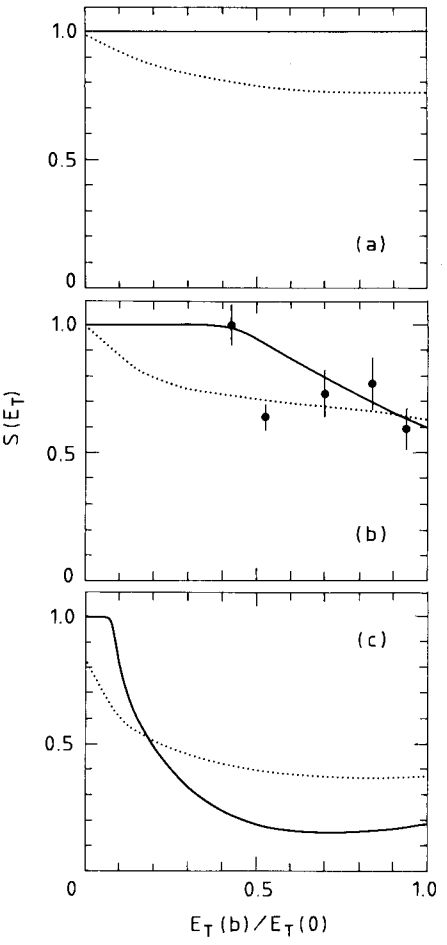

Fig. 8a, b. The E_T dependence of J/ψ suppression for S–S **a**, S–Pb **b** and Pb–Pb collisions at the SPS. Shown are the predictions from colour screening (solid line) and from absorption (dotted line); the data in **b** are from [11]

In both cases it is evident that the present data cannot distinguish between the different suppression mechanisms. It is also clear that besides a general increase in statistics, the most useful further data would be at high P_T (for the P_T dependence) and at low E_T (for the E_T dependence). Moreover it should be noted that colour screening does not lead to any suppression for S–S collisions, whereas absorption together with initial state parton scattering predicts about 35% suppression at $P_T=0$. Such an experiment is presently possible at the CERN-SPS and would in addition be of interest also for a comparison with the planned symmetric Pb–Pb collisions. From Figs. 7c and 8c we conclude that it will be difficult to distinguish the different mechanisms on the basis of Pb–Pb collisions alone.

The behaviour of the ratio of ψ' to J/ψ production as function of E_T and P_T has so far not been studied experimentally in a statistically significant way, but data on this are presently under analysis. In Fig. 9 we show the patterns predicted by the different mechanisms; we have normalised our results such that the ratio is unity for the case of no suppression. In Fig. 9a we see again that there is a noticeable difference between the predictions from deconfinement and absorption for S–S col-

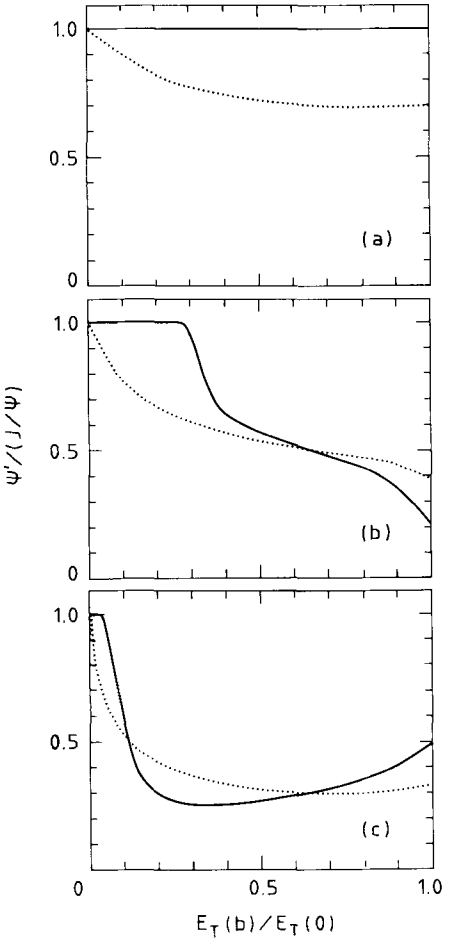

Fig. 9a, b. The E_T dependence of the ratio of ψ' to J/ψ production for S–S **a**, S–Pb **b** and Pb–Pb collisions at the SPS. Shown are the predictions from colour screening (solid line) and from absorption (dotted line). The ratios are normalised to unity for no suppression

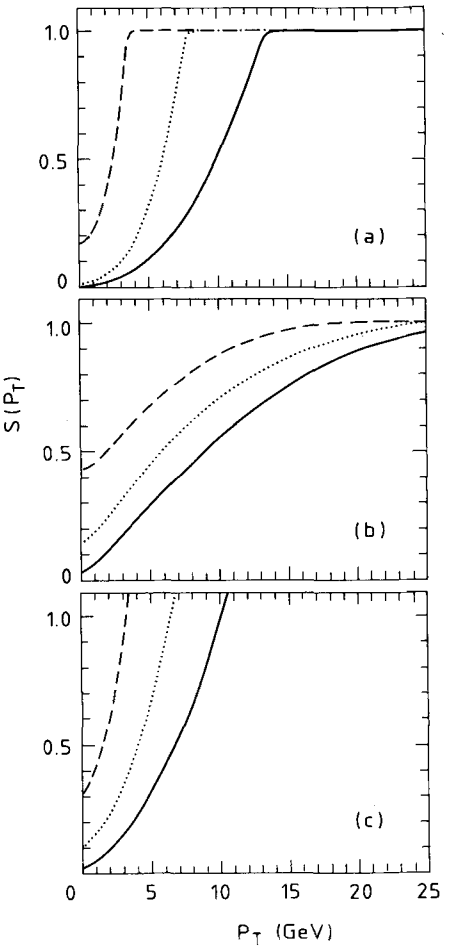

Fig. 10a–c. The P_T dependence of ψ suppression for Pb–Pb collisions at SPS (dashed line), RHIC (dotted line), and LHC (solid line). Shown are the predictions from colour screening **a**, from absorption **b**, and from absorption with initial state scattering **c**

lisions: at SPS energy, neither J/ψ nor ψ' experiences any suppression due to colour screening. In contrast to this, we find in Fig. 9c for Pb–Pb collisions rather little difference between the different mechanisms. – Figure 9b illustrates once more how useful data at low energy density would be.

How do the suppression patterns change with increasing incident energy? In Fig. 10 we show the P_T dependence of ψ suppression in Pb–Pb collisions at SPS, RHIC and LHC energies, for the different scenarios considered. Here we have shown the behaviour of the directly produced ψ's, since the amount of production through decay from excited $c\bar{c}$ states at very high energies still has to be determined [56]. The same caveat applies to the P_T distributions for the Υ, shown in Fig. 11 for LHC energy.

Next we compare in Fig. 12 the E_T dependence of ψ and Υ suppression for S–S and Pb–Pb collisions at the LHC. The most striking feature here is the complete absence of suppression by colour screening for both S–S and Pb–Pb collisions, in contrast to more than 50% suppression by absorption in the Pb–Pb case. It must be emphasized, however, that this effect is of practical use only if there exists a P_T region in which direct Υ production provides a sizeable fraction of the observed dilepton pairs, since both Υ'' and χ_b production are suppressed by deconfinement.

The abrupt onset of suppression in ε, and its abrupt end in P_T, as obained from colour screening, is a consequence of the sharp formation time of the bound states in question. If the deconfining medium were present already at time $t=0$, then we would have to study the evolution of the bound state for a screened potential, and this considerably softens both the ε and the P_T distributions [29–31]. On the other hand, it will take some time before the $c\bar{c}$ or $b\bar{b}$ pair can experience an effect of the medium, and even longer time for the plasma to become established. Hence the distributions we have shown should given an indication of the expected behaviour, even though they will be softened somewhat.

Finally we want to comment briefly on how the average transverse momentum of the produced charmonium and bottonium states depends on E_T for colour screening and for initial state parton scattering. We had seen that

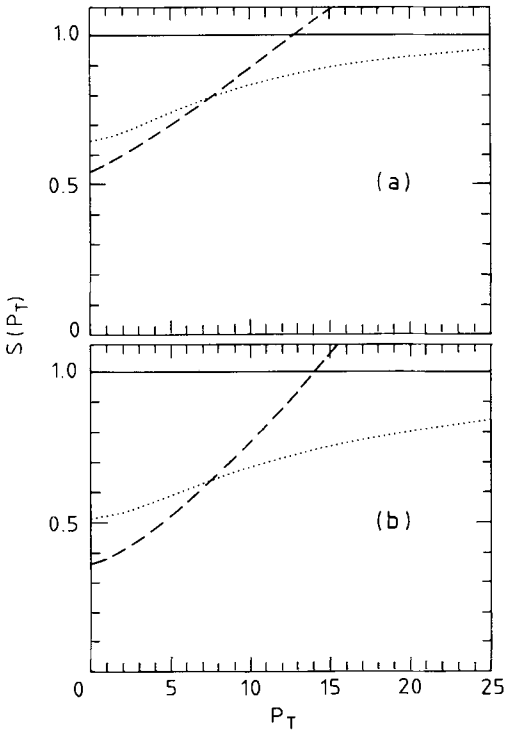

Fig. 11a, b. The P_T dependence of Υ suppression for S−S **a** and Pb−Pb **b** collisions at the LHC. Shown are the predictions from colour screening (solid line), from absorption (dotted line), and from absorption with initial state scattering (dashed line)

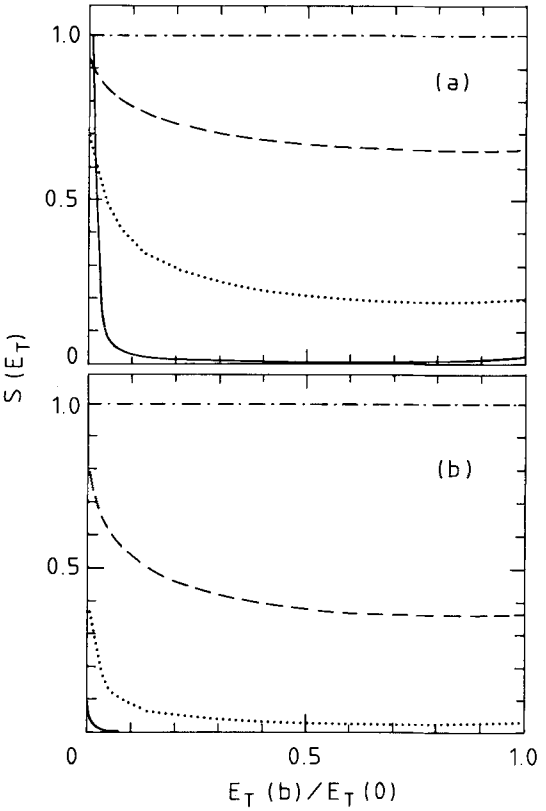

Fig. 12a, b. The E_T dependence of ψ and Υ suppression for S−S **a** and Pb−Pb **b** collisions at the LHC. Shown are the predictions from colour screening (ψ: solid line, Υ: dash-dotted line) and from absorption (ψ dotted line, Υ: dashed line)

$\langle P_T \rangle$ depends on ε for the former and on E_T for the latter; we had also noted, in Fig. 6, that for asymmetric collisions ($A \ll B$), ε increases with E_T, whereas in symmetric collisions ($A-A$), ε remains approximately constant over most of the E_T range. As a consequence, the variation of $\langle P_T \rangle$ with E_T is quite different in the two situations, if we have colour screening. In $A-B$ collisions, $\langle P_T \rangle$ increases almost linearly with E_T, once the deconfinement threshold is passed; in $A-A$ collisions, $\langle P_T \rangle$ remains approximately independent of E_T once we are past the threshold. For initial state parton scattering, on the other hand, there is no essential difference between the two cases, and we always have $\langle P_T \rangle$ increasing with E_T in a form given by (43).

6 The experimental feasibility of a spectral analysis of strongly interacting matter

In this section, we want to consider briefly the conditions necessary to carry out an analysis of the type we have proposed and to mention some of the difficulties that will arise.

We define here the signal above the Drell-Yan continuum as the intensity of our spectral lines, i.e., as the quantity we expect to vary with energy density or temperature [5]. In doing so, we assume that the overall Drell-Yan production in nuclear collisions around $y=0$ does not experience any nuclear effects. This is in accord with all $p-A$ data so far, which give $A^{-1}\mathrm{d}^2\sigma/\mathrm{d}M^2\mathrm{d}y = \mathrm{d}^2\sigma_0/\mathrm{d}M^2\mathrm{d}y$; i.e., suitably normalised, $p-A$ data agree with those from $p-p$ collisions.

Since the Drell-Yan distributions are thus used to calibrate the measurement of the signal, they are a prerequisite for a spectral analysis. The overall Drell-Yan cross-section can be estimated by the (dimensionless) scaling form [57] used in $p-p$ collisions,

$$M^4(\mathrm{d}^2\sigma/\mathrm{d}M^2\mathrm{d}y)_{y=0} \simeq 3.75\times 10^{-5}\exp\{-15\sqrt{\tau}\}, \qquad (45)$$

which fits all existing data. To obtain the rates for *central* $A-A$ collisions, we simply multiply by A^2. Scaling violations are expected to increase the yield somewhat [54], while nuclear shadowing will decrease it by up to 50% at high energies [58]. Neglecting these effects, we get the cross-sections and rates shown in Table 4; similar results for RHIC energy are obtained in [15]. Given

Table 4. Drell-Yan cross-sections and monthly production rates

Energy	SPS	RHIC	LHC
$\mathscr{L}$ [cm^{-2} s^{-1}]	10^{28}	10^{26}	10^{27}
$(\mathrm{d}\sigma/\mathrm{d}M^2\mathrm{d}y)_{y=0}^{M=4}\left[\frac{\mathrm{mb}}{\mathrm{GeV}^2}\right]$	7.6×10^{-5}	1.9×10^{-3}	2.5×10^{-3}
$(\mathrm{d}\sigma/\mathrm{d}M^2\mathrm{d}y)_{y=0}^{M=9}\left[\frac{\mathrm{mb}}{\mathrm{GeV}^2}\right]$	3.5×10^{-8}	5.2×10^{-5}	9.6×10^{-5}
((events/GeV)/month)$_{y=0}^{M=4}$	1.6×10^{4}	3.9×10^{3}	5.2×10^{4}
((events/GeV)/month)$_{y=0}^{M=9}$	1.6×10^{1}	2.5×10^{2}	4.5×10^{3}

good data over a fairly large mass range, say between $M=4$ and 7 GeV, one might consider extrapolating to the $b\bar{b}$ region to obtain the continuum there, if statistics become too low at $M \simeq 9$–10 GeV.

The energy dependence of $c\bar{c}$ and $b\bar{b}$ resonances is phenomenologically [57, 59] described by the same form as Drell-Yan production,

$$M_x^4 (\mathrm{d}\sigma_x/\mathrm{d}y)_{y=0} = \simeq 3.75 \times 10^{-5} b_x \exp\{-15\sqrt{\tau_x}\}, \quad (46)$$

with $\tau_x \equiv M_x/\sqrt{s}$ and a normalisation b_x to be determined empirically. Data [57, 60] indicate $b_{J/\psi} \sim 120$, $b_{\psi'} \sim 4$, $b_\Upsilon \sim 30$. To get some idea of the expected $c\bar{c}$ and $b\bar{b}$ bound state production rates, we can therefore multiply the Drell-Yan rates by the corresponding factor. On the other hand, the restriction to central collisions and corrections for experimental acceptances will reduce the rates by at least a factor 10, perhaps by 10^2. Thus it is clear that the luminosity of the planned high energy colliders RHIC and LHC is an absolutely crucial factor for a full spectral analysis of $c\bar{c}$ and $b\bar{b}$ states.

In view of this, we should also note that although Drell-Yan and $Q\bar{Q}$ resonance production cross sections drop with decreasing A, the luminosity increases [61, 62], and it is thus conceivable that beams with $A \simeq 100$ may lead to higher rates than Pb beams.

We had seen in the discussion of the presently available SPS data, that for a full analysis it is necessary to have data over a wide range of energy densities, not just at the peak values. On the other hand, for symmetric $(A-A)$ collisions E_T variations do not lead to significant energy density variations, as we saw in Fig. 5. Hence it is in fact necessary to run either at different energies or at different A. Although the former is in principle preferable, since the initial volume is kept constant, it appears to be technically difficult [63]. Hence for this reason as well, the possibility to study $A-A$ collisions for different A becomes essential. The variation of the average energy density with A in $A-$Pb and $A-A$ collisions is shown in Fig. 13 for SPS energy. We see that

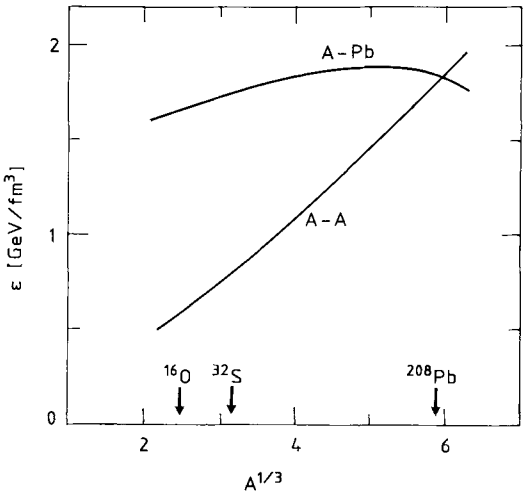

Fig. 13. The A dependence of the average energy density ε in $A-A$ and $A-$Pb collisions

by going from O–O to Pb–Pb collisions, the energy density increases from well below the deconfinement point to values almost twice ε_c; in contrast, the change between S–Pb and Pb–Pb is at most around 10%. Incidentally, the variation of ε for $S-A$ collisions, i.e., for fixed beam and varying target, is essentially identical to that for $A-A$ collisions. Hence a study of charmonium suppression using a sulphur beam on different targets would cover the whole range of average energy densities possible at the SPS. Unfortunately this is technically not so simple, since the center of mass will change with A.

Furthermore we can estimate from Fig. 13 the threshold value of A in $A-A$ collisions, at which J/ψ suppression begins. From Fig. 2a, we note that ψ suppression starts at $\varepsilon \simeq 1.9$ GeV/fm^3; since χ_c suppression begins at a somewhat higher value, this determines the suppression threshold. From Fig. 6, we conclude that the peak energy density in the interior of the interaction region is about 1.7 times the average value, so that J/ψ suppression should start when the average energy density becomes about 1.1 GeV/fm^3. From Fig. 13, we see that this is the case for $A \simeq 64$, i.e., for copper-copper collisions.

Finally we want to mention briefly a problem that will arise once detailed data for charmonium and bottonium production at very high energies are analysed. The amount of directly produced J/ψ compared to that from χ_c decay is quite strongly P_T dependent [56], and this has to be taken into account in the actual predictions. In addition, at Tevatron energy ($\sqrt{s}=1.8$ TeV), the production of J/ψ for $P_T \geqq 6$–7 GeV is dominated by production through B decay [27]; for higher $\sqrt{s}$, the range not contaminated by decay becomes even smaller. At RHIC energy, however, B decay contributions begin to dominate only for $P_T \geqq 10$ GeV. A study of the P_T limit of J/ψ suppression (see Fig. 10) will thus become difficult above RHIC energies.

7 Conclusions

The spectral analysis of $c\bar{c}$ and $b\bar{b}$ bound states in the dilepton emission from high energy heavy ion collisions appears to provide a powerful and experimentally feasible tool to study the primordial state of the systems produced in these collisions. The evolution of the suppression with increasing A and increasing cms energy, together with suppression limits in P_T, should tell us much about the energy densities and hence about the temperatures achieved in the collision. Since both absorption and colour screening will presumably occur even in the absence of full equilibrium, it seems essential that complementary experiments, such as the study of particle ratios, provide information about this aspect. Moreover, it would be very useful if the geometric arguments, used in obtaining the variation of suppression with both A and impact parameter b, could be reinforced by interferometry measurements.

In closing, we summarize the main features that could provide a tool to check if high energy heavy ion experiments do in fact produce a quark-gluon plasma.

Colour screening does not lead to any J/ψ or ψ' suppression for S – S collisions at SPS energy, where absorption already gives about 35% suppression at small P_T. Similarly, in the deconfinement picture there is no suppression of *direct* Υ production up to LHC energy, where absorption leads to more than 50% suppression of the direct channel.

Colour screening leads in general to a more abrupt onset of suppression than absorption, both in E_T and in P_T. This implies differences not just for values of ε below the deconfinement threshold; it also results in less suppression by absorption at high ε. Thus in a deconfinement picture, the J/ψ is in effect completely suppressed at RHIC energy and above; in contrast, it should survive up to 25% or so even at the LHC, if absorption causes the suppression.

The variation of the average transverse momentum of the $c\bar{c}$ and $b\bar{b}$ bound states as function of E_T provides a further possible tool. For $A-B$ collisions, colour screening and initial state parton scattering lead to a similar E_T-dependence of $\langle P_T \rangle$; for $A-A$ collisions, however, ε does not vary significantly with E_T, and hence $\langle P_T \rangle$ becomes essentially E_T-independent for colour screening, while it continues to rise with E_T for initial state parton scattering.

Finally, we recall that colour screening has an effect at high energy densities only on $c\bar{c}$ and $b\bar{b}$ states, not on Drell-Yan pairs [45]; initial state parton scattering, on the other hand, leads to a strong E_T-dependence of the P_T distributions for Drell-Yan pairs as well.

We therefore expect that a complete spectral analysis of $c\bar{c}$ and $b\bar{b}$ states, together with a study of Drell-Yan pairs, will provide better understanding of the nature of dense strongly interacting matter.

Acknowledgements. It is a pleasure to thank the members of the LHC Heavy Ion Working Group, in particular S. Gupta and U. Heinz, for many stimulating discussions.

References

1. See e.g.: Proceedings of Quark Matter '88, Nucl. Phys. A498 (1989)
2. See e.g.: M. Gyulassy: Nucl. Phys. A418 (1985) 559c, and references given there
3. R. Albrecht et al. (WA80): Upper Limit for Thermal Direct Photon Production in Heavy Ion Collisions at 60 and 200 A – GeV, Preprint CERN-PPE/91-01, 1991
4. See e.g., V. Ruuskanen, in: Proceedings of the VIIIth International Conference on Ultra-Relativistic Nucleus-Nucleus Collisions, Menton/France, 1990; Nucl. Phys. A, in press
5. T. Matsui, H. Satz: Phys. Lett. 178B (1986) 416
6. F. Karsch, R. Petronzio: Phys. Lett. 193B (1987) 105
7. M.C. Abreu et al. (NA38): Z. Phys. C – Particles and Fields 38 (1988) 117
8. L. Kluberg (NA38): Nucl. Phys. A488 (1988) 613c
9. J.Y. Grossiord (NA38): Nucl. Phys. A498 (1989) 249c
10. C. Baglin et al. (NA38): Phys. Lett. 220B (1989) 471
11. O. Drapier (NA38): Dépendence en impulsion transverse de la production du J/ψ dans les interactions $p-$U, O – U et S – U á 200 GeV/c par nucléon, Thesis, University of Lyon, May 1990
12. J. Ftáčnik, P., Lichard, J. Pišút: Phys. Lett. B207 (1988) 194
13. C. Gerschel, J. Hüfner: Phys. Lett. 207B (1988) 253
14. S. Gavin, M. Gyulassy, A. Jackson: Phys. Lett. 207B (1988) 257
15. R. Vogt, M. Prakash, P. Koch, T.H. Hansson: Phys. Lett. 207B (1988) 263
16. J. Ftáčnik, P. Lichard, N. Pišútová, J. Pišút: Z. Phys. C42 (1988) 139
17. J. Blaizot, J.Y. Ollitrault: Phys. Rev. D39 (1989) 232
18. S. Gavin, M. Gyulassy: Phys. Lett. B214 (1988) 241
19. J. Hüfner, Y. Kurihara, H.J. Pirner: Phys. Lett. 215B (1988) 218
20. J. Blaizot, J.Y. Ollitrault: Phys. Lett. 217B (1989) 392
21. J. Blaizot, J.Y. Ollitrault: Phys. Lett. 199B (1987) 499
22. F. Karsch, R. Petronzio: Phys. Lett. B212 (1988) 255
23. F. Karsch, R. Petronzio: Z. Phys. C – Particles and Fields 37 (1988) 627
24. M.-C. Chu, T. Matsui: Phys. Rev. D37 (1988) 1851
25. See e.g., K. Kajantie, Nucl. Phys. A498 (1989) 355c, and R. Kippenhahn, A. Weigert: Stellar Structure and Evolution. Berlin Heidelberg New York: Springer 1990
26. Y. Lemoigne et al.: Phys. Lett. 113B (1982) 509
27. E.W.N. Glover et al.: Z. Phys. C – Particles and Fields 38 (1988) 473
28. F. Karsch, M.T. Mehr, H. Satz: Z. Phys. C – Particles and Fields 37 (1988) 617
29. T. Matsui: Ann. Phys. (NY) 196 (1989) 182
30. J. Cleymans, R.L. Thews: Z. Phys. C – Particles and Fields 45 (1990) 391
31. V. Cerny et al.: Z. Phys. C – Particles and Fields 46 (1990) 481
32. S.J. Brodsky, A.H. Mueller: Phys. Lett. B206 (1988) 685
33. S. Jacobs, M.G. Olsson, C. Suchyta III: Phys. Rev. D33 (1986) 3338
34. P.V. Ruuskanen, H. Satz: Z. Phys. C – Particles and Fields 37 (1988) 623
35. See e.g.: B. Petersson, in: Proceedings of the VIIIth International Conference on Ultra-Relativistic Nucleus-Nucleus Collisions, Menton/France, 1990; Bielefeld Preprint BI-TP 90/28; Nucl. Phys. A, in press
36. J.D. Bjorken: Phys. Rev. D27 (1983) 140
37. R. Hwa, K. Kajantie: Phys. Rev. D32 (1985) 1109
38. M. Gyulassy, in: Multiparticle Dynamics, P. Yager, J.F. Gunion (eds.). Singapore: World Scientific 1984
39. H. Satz, in: Proceedings of the Large Hadron Collider Workshop, G. Jarlskog, D. Rein (eds.), Vol. I, 188; CERN 90-10, 1990
40. J. Badier et al.: Z. Phys. C – Particles and Fields 20 (1983) 101
41. B. Povh, J. Hüfner: Phys. Rev. Lett. 58 (1987) 1612
42. C. Michael, G. Wilk: Z. Phys. C – Particles and Fields 10 (1981) 169
43. G.T. Bodwin et al.: Phys. Rev. Lett. 47 (1981) 1799
44. P. Chiappetta, H.J. Pirner: Nucl. Phys. B291 (1987) 765
45. H. Satz: Phys. Lett. 242B (1990) 107
46. See e.g.: G.R. Young (WA80): Nucl. Phys. A498 (1989) 53c
47. A. Kaidalov: Nucleus-nucleus interaction dynamics and the Glauber-Gribov approach, Preprint CERN-TH.5781/90, 1990
48. See e.g.: H. Ströbele, in: Proceedings of the VIIIth International Conference on Ultra-Relativistic Nucleus-Nucleus Collisions, Menton/France, 1990; Nucl. Phys. A, in press
49. U. Heinz, P. Koch, B. Friman: in: Proceedings of the Large Hadron Collider Workshop, G. Jarlskog, D. Rein (eds.), Vol. II
50. F. Abe et al. (CDF): Phys. Rev. D41 (1990) 2330
51. See e.g.: C. Grosso-Pilcher, M. Shochet: Ann. Rev. Nucl. Part. Sci. 36 (1986) 1, and references given there
52. P. Chiappetta, M. Greco: Nucl. Phys. B221 (1983) 269
53. See e.g.: G. Altarelli, R.K. Ellis, G. Martinelli: Phys. Lett. 151B (1985) 457
54. S. Gupta, in: Proceedings of the Large Hadron Collider Workshop, G. Jarlskog, D. Rein (eds.), Vol. II
55. F. Karsch, in: Proceedings of the Large Hadron Collider Workshop, G. Jarlskog, D. Rein (eds.), Vol. II

56. L. Bergström, R.W. Robinett, L. Weinkauf: Phys. Rev. D42 (1990) 825
57. N.S. Craigie: Phys. Rep. 47 (1978) 1
58. P. Castorina, in: Proceedings of the Large Hadron Collider Workshop, G. Jarlskog, D. Rein (eds.), Vol. II
59. T.K. Gaisser, F. Halzen, E.A. Paschos: Phys. Rev. D15 (1977) 2572
60. R. Vogt: Rate Estimates for Vector Meson and Drell-Yan Production in Relativistic Heavy Ion Collisions, Livermore Preprint UCRL-JC-105057, 1990
61. D. Brandt: Relativistic Heavy Ions in the LHC, CERN LHC Note No. 87, 1990
62. Conceptual Design of the RHIC, BNL 52195, 1989
63. D. Brandt, private communication